

## CONTROLLED CHANGES IN SPECTRA OF OPEN QUASI-OPTICAL RESONATORS

L. G. Velychko and Y. K. Sirenko

Institute of Radiophysics and Electronics  
National Academy of Sciences of Ukraine  
12 Acad. Proskura St., Kharkov 61085, Ukraine

**Abstract**—The efficiency of different ways for controlled changes of spectral characteristics of open electrodynamic resonant structures are studied and evaluated in the paper.

### 1. INTRODUCTION

Free electromagnetic oscillations in a quasi-optical open resonator, i.e., in a resonator whose basic dimensions are much greater than the operating wavelength  $\lambda = 2\pi/k$ , are generated by the beams of plane waves propagating in opposite directions between resonator's mirrors. By moving along the closed paths, the beams recover their phase characteristics when returning at some fixed point thus ensuring stability of the field pattern.

There exist many ways for changing spectral characteristics of resonators with simple dielectric or metal mirrors [1]. Thus for example, a low-sized scattering object being placed in the antinode of some high-Q oscillation destroys this oscillation. The corresponding complex eigenfrequency  $\bar{k}$  vanishes from the spectral set  $\Omega_k$  (pure spectrum sparseness). By changing mirror's curvature, one can control a degree of beams defocusing, and hence, the Q-factor of the corresponding oscillations. In such a situation, with slight growth (reduction) in  $|\text{Im}\bar{k}|$  we can observe actual sparseness (crowding) of the spectrum — nominally the eigenfrequencies  $\bar{k}$  keep their places in the spectral set  $\Omega_k$  but the actual 'status' of the oscillations decreases (increases) substantially. A similar result can be obtained by varying the mirror transmission or reflectivity. Through rotating the mirrors or replacing the flat mirrors by the mirrors of curved or broken shape,

---

Corresponding author: L. G. Velychko (lgv@ire.kharkov.ua).

one can break the beam trajectory and force the beam to leave the resonator (pure spectrum sparseness).

With slight mirror shifts leaving the beam traveling direction unchanged or with small variations in the mirror transmission or reflectivity, elements  $\bar{k}$  of the spectral set  $\Omega_k$  change insignificantly within a frequency band  $k \in [K_1; K_2]$  as does the free oscillation pattern. At the same time, the slight variations in geometric or material parameters of this kind may cause anomalously abrupt changes of the resonator spectral characteristics. This is the case, for example, when the eigenfrequencies of the oscillations of the common symmetry class approach closely in the metric of the complex space to which these eigenfrequencies belong [2, 3].

The approach based on a replacement of simple mirrors with selective grating-mirrors is found to be quite efficient in the controllable changes of open resonator spectra. A close look at the mode-selection mechanism in open resonators with diffraction gratings as resonator's mirrors were started in [2], where a practically feasible approach was suggested to the problem of synthesizing a 2-D resonator with essentially sparse spectrum and given electromagnetic characteristics at the operating wavelength. The essence of the approach is as follows. A prototype (an open or closed quasi-optical resonator) with easily analyzable spectral characteristics such as a set  $\Omega_k^{prot}$  of eigenfrequencies  $\bar{k}_n$  and associated free oscillations  $\bar{U}(g, \bar{k}_n)$ ,  $g = \{y, z\} \in \mathbf{R}^2$ , is selected. One of the nonselective mirrors is replaced with a grating mirror such that the free oscillation of the prototype resonator associated with the chosen eigenfrequency  $\bar{k} \in \Omega_k^{prot}$  is conserved. To perform this replacement, it is necessary that the nonselective mirror and the grating mirror being illuminated by plane waves (the partial components of  $\bar{U}(g, \bar{k})$ ) behave identically. In this case, the frequency  $\bar{k} \in \Omega_k^{prot}$  belongs also to the set  $\Omega_k^{mod}$  of eigenfrequencies of the modified resonator. The other elements of the set  $\Omega_k^{mod}$  satisfy the overdetermined system of dispersion equations consisting of the modified dispersive equations for the prototype and the relations whose satisfaction is required for maintenance of stable oscillations in the open resonator with a diffraction grating. This system includes complex amplitudes  $A_n$  and  $B_n$  ( $n = 0, \pm 1, \pm 2, \dots$ ) of spatial harmonics of the grating [4, 5] as a function of  $k$  and of the angle of arrival of primary plane waves; the incident plane waves together with the waves composing the secondary field are considered as partial components of a free oscillation in the open resonator. The system is overdetermined. This fact ensures the evident essential spectrum sparseness of the modified dispersive resonator. Another

way for cutting the set  $\Omega_k^{mod}$  is to reduce Q-factor of the remaining free oscillations. The values of  $A_n$  and  $B_n$  in the range under consideration determine how effectively these additional abilities are realized. Taken together these factors cutting the set  $\Omega_k^{mod}$  constitute the oscillation selection mechanism in the synthesized open resonator. Under reasonable use of various resonant and nonresonant scattering modes of diffraction gratings [2, 4, 5], this mechanism can be very efficient.

The approach based on the prototype principle was realized in [6, 7], where the time-domain methods were used for accurate calculation and optimization of basic characteristics and parameters for a few open 2-D resonators with grating mirrors. In Section 4, we continue this study and present numerical results in the controlled changes of spectra of some 2-D quasi-optical resonators. Section 3 deals with the same problems with special emphasis on the testing of the standard ways for controlled spectrum changes, which have received mention in the literature (for example, [1]) but whose efficiency has not yet been estimated. Section 2 briefly discusses the models and previously obtained results used in our study.

In this work, rigorous time-domain approaches based on the standard finite-difference algorithms [8] with the original exact absorbing conditions [3, 9] are applied. The technique of this kind allows one to obtain reliable results when investigating long-duration transient processes. Spectral problems are the problems of the frequency domain. To solve them by the time-domain methods, we apply a special technique developed in [6, 7] and based on the realization of analytic relations between space-time and space-frequency characteristics of forced and free electromagnetic oscillations in open electrodynamic structures. Analysis in the frequency domain in our case requires incomparably greater calculating time, especially when studying objects of resonant quasi-optics (for example, open resonators with grating mirrors) whose characteristic dimensions differ by an order or more.

## 2. FORMULATION

Amplitudes of the free oscillation  $\bar{U}(g, \bar{k})$  decreases as  $\exp(t\text{Im}\bar{k})$ . High-Q free oscillations ( $Q = \text{Re}\bar{k}/2|\text{Im}\bar{k}| \gg 1$ ) decay very slowly; therefore to obtain reliable results when determining amplitude-frequency characteristics of some resonant object by time-domain methods one should substantially extend the observation time interval  $0 \leq t \leq T$  [6, 7]. As a consequence, transient processes under resonant conditions (and of course, the associated steady-state processes) can

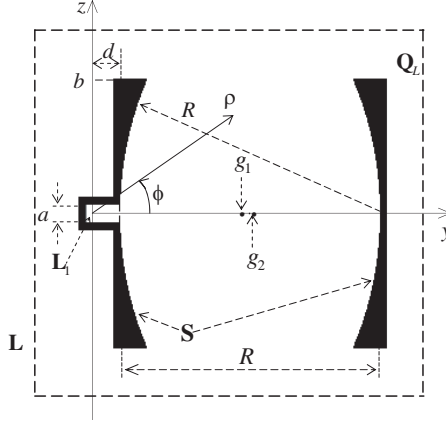


**Figure 1.** A confocal resonator with a waveguide input ( $R = 9.0$ ,  $b = 4.0$ ,  $a = 0.56$ ,  $d = 1.2$ ) and general geometry of model initial boundary-value problems (1). The point  $g_2 = \{5.7, 0.0\}$  is located at the center of the resonator.

be analyzed by those time-domain methods whose computational error is not high both for small and for large values of  $t$ . This requirement is met by the standard finite-difference algorithms [8] whose computational domain is truncated by the original exact absorbing conditions [3, 9].

We consider 2-D model initial boundary-value problems (Fig. 1)

$$\left\{ \begin{array}{ll} \left[ -\varepsilon(g) \frac{\partial^2}{\partial t^2} - \sigma(g) \frac{\partial}{\partial t} + \frac{\partial^2}{\partial y^2} + \frac{\partial^2}{\partial z^2} \right] U(g, t) = F(g, t), & g = \{y, z\} \in \mathbf{Q}, \quad t > 0 \\ U(g, t)|_{t=0} = \frac{\partial}{\partial t} U(g, t)|_{t=0} = 0, & g \in \overline{\mathbf{Q}} \\ D[U(g, t) - U^i(g, t)]|_{g \in \mathbf{L}_1} = 0, & t \geq 0 \\ U(g, t)|_{g \in \mathbf{S}} = 0 & t \geq 0 \end{array} \right. \quad (1)$$

describing transient states of the  $E$ -polarized field:  $E_y = E_z = H_x \equiv 0$ ,  $U(g, t) = E_x(g, t)$ ,  $\partial H_y / \partial t = -\eta_0^{-1} \partial E_x / \partial z$ ,  $\partial H_z / \partial t = \eta_0^{-1} \partial E_x / \partial y$ . The field is generated by the waves  $U^i(g, t)$  arriving from an input waveguide  ${}_1\mathbf{Q}$  onto a boundary  $\mathbf{L}_1$  ( $F(g, t) \equiv 0$ ) or by the current sources  $F(g, t)$  (the structure is free from the input waveguide  ${}_1\mathbf{Q}$ ). Metal and dielectric objects (the elements of the open resonator) are located in the bounded region  $\mathbf{Q}_L \subset \mathbf{Q}$  of the plane  $\mathbf{R}^2$  of variables  $y$  and  $z$ . Here  $\vec{E} = \{E_x, E_y, E_z\}$  and  $\vec{H} = \{H_x, H_y, H_z\}$  are the electric and magnetic field vectors;  $\sigma = \eta_0 \sigma_0$ ;  $\eta_0 = (\mu_0 / \varepsilon_0)^{1/2}$  is the impedance

of free space;  $\varepsilon_0$  and  $\mu_0$  are the electric and magnetic constants of vacuum;  $\varepsilon \equiv \varepsilon(g) \geq 1$  is the relative permittivity and  $\sigma_0 \equiv \sigma_0(g) \geq 0$  is the specific conductivity of the locally inhomogeneous medium. The domain under study  $\mathbf{Q}$  is the part of the  $\mathbf{R}^2$ -plane bounded by the contours  $\mathbf{S}$  and the boundary  $\mathbf{L}_1$ , where  $\mathbf{S} \times [|x| \leq \infty]$  is a surface of perfect conductors. The finite in the closure of  $\mathbf{Q}$  functions  $F(g, t)$ ,  $\sigma(g)$ , and  $\varepsilon(g) - 1$  are assumed to satisfy the theorem on unique solvability of problems (1) in the Sobolev space  $\mathbf{W}_2^1(\mathbf{Q}^T)$ ,  $\mathbf{Q}^T = \mathbf{Q} \times (0; T)$ ,  $T < \infty$  (see Statement 1 in [7]). In the paper, the SI system of units is used. The variable  $t$  is the product of the real time by the velocity of light in free space and has the dimensions of length.

The region  ${}_L\mathbf{Q} = \mathbf{Q} \setminus (\mathbf{Q}_L \cup \mathbf{L})$  ( $\mathbf{L}$  is the outer boundary of  $\mathbf{Q}_L$ ) is free from sources and scatterers, but they are allowable in the semi-infinite virtual parallel-plate waveguide  ${}_1\mathbf{Q}$  adjacent to the domain  $\mathbf{Q}_L$  along the boundary  $\mathbf{L}_1$ . Introduction of a waveguide of this kind allows the objects with infinite regular metal boundaries to be simulated in the context of more convenient and physically based conception, which holds, strictly speaking, only for compact inhomogeneities of free space.

The unbounded domain  $\mathbf{Q}$  in (1) is truncated to a bounded domain  $\mathbf{Q}_L$  with the help of the exact local absorbing conditions constructed in [3, 9]. The condition like (4.31) from [3] is used on the boundary  $\mathbf{L}_1$  in a cross-section of the virtual waveguide  ${}_1\mathbf{Q}$  (see equation  $D[U(g, t) - U^i(g, t)]|_{g \in \mathbf{L}_1} = 0$  in (1)), whereas on the rectangular boundary  $\mathbf{L}$  we use condition (3.28)–(3.30) from [3]. Thus by setting on the boundary  $\mathbf{L}_1$  the amplitudes of the waves  $U^i(g, t)$  generated by the sources whose supports are located in the virtual domain  ${}_1\mathbf{Q}$ , we can simulate the excitation of the structure from an input waveguide.

Let the structure shown in Fig. 1 be excited by a current source  $F(g, t)$  or by a signal  $U^i(g, t) = U_p^i(g, t) = v_p(y, t) \mu_p(z)$  with  $p \geq 1$  ( $H_{0p}$ -wave) from the virtual input waveguide. In this case, a total field  $U(g, t)$  in the region  ${}_1\mathbf{Q}$  can be written as

$$U(g, t) = U_p^i(g, t) + U^s(g, t) = v_p(y, t) \mu_p(z) + \sum_{n=1}^{\infty} u_n(y, t) \mu_n(z), \quad (2)$$

where  $\{u_n(z, t)\}$  is the evolutionary basis [3] of the signal  $U^s(g, t)$  generated by inhomogeneities of the path and crossing the boundary  $\mathbf{L}_1$  in  $y \rightarrow -\infty$  direction,  $\{\mu_n(z)\}$  is a system of the orthonormal transverse functions  $\mu_n(z) = \sqrt{2/a} \sin[n\pi(z - \underline{z})/a]$ ,  $a = \bar{z} - \underline{z}$  stands for the waveguide height,  $z = \underline{z}$  and  $z = \bar{z}$  are the planes in which the bottom and upper waveguide wall lies.

For the radiation zone we obtain ( $\rho$  and  $\phi$  are the polar coordinates)

$$U(g, t) = U(\rho, \phi, t) = \sum_{n=-\infty}^{\infty} \bar{u}_n(\rho, t) \bar{\mu}_n(\phi), \quad \rho \geq L, \quad 0 \leq \phi \leq 2\pi, \quad (3)$$

where  $\rho = L$  is the circle lying entirely in  $\mathbf{Q}_L$  and enveloping all inhomogeneities of  $\mathbf{R}^2$ -space and all sources  $F(g, t)$ ,  $\bar{\mu}_n(\phi) = (2\pi)^{-1/2} \exp(in\phi)$  ( $n = 0, \pm 1, \pm 2, \dots$ ) is the complete system of transverse functions, and  $\bar{u}_n(\rho, t)$  are the space-time amplitudes forming the evolutionary basis  $\{\bar{u}_n(\rho, t)\}$  of the outgoing wave  $U(\rho, \phi, t)$  (see, for example, Section 3.2 in [3]).

A finite-difference algorithm for solving problems (1) supplemented with the exact absorbing conditions on the boundaries  $\mathbf{L}_1$  and  $\mathbf{L}$  [3, 9] is implemented in a software package for computing key space-time and space-frequency characteristics of the open electrodynamic structures considered. Certain of these characteristics are listed below.

- Space-time and space-frequency distribution  $E_x(g, t)$  ( $T_1 \leq t \leq T_2 \leq T$ ) and  $\tilde{E}_x(g, k)$  ( $K_1 \leq k \leq K_2$ ) in the domain  $\mathbf{Q}_L$ .
- The energy  $W_{np}(k)$  ( $K_1 \leq k \leq K_2$ ) of the  $H_{0n}$ -mode reflected back into the input waveguide  ${}_1\mathbf{Q}$  when exciting the open resonator by the  $H_{0p}$  propagating wave.
- Normalized radiation pattern

$$D(\phi, k, M) = \frac{\left| \tilde{U}(M, \phi, k) \right|^2}{\max_{\phi_1 < \phi < \phi_2} \left| \tilde{U}(M, \phi, k) \right|^2}, \quad K_1 \leq k \leq K_2 \quad (4)$$

on the section  $0 \leq \phi_1 \leq \phi \leq \phi_2 \leq 360^\circ$  of the arch  $\rho = M \geq L$  enveloping all sources and inhomogeneities of the  $\mathbf{R}^2$ -space,  $K_1 \leq k \leq K_2$ . The main lobe is directed at the angle  $\phi(k)$ ,  $D(\phi(k), k) = 1$ .  $\phi_{0.5}(k)$  is the lobe width on the level of  $D(\phi, k) = 0.5$ .

- Radiation efficiency  $\eta(k) = 1 - \sum_n W_{np}(k)$  on the frequency  $k$  (for  $F(g, t) = 0$  and  $\sigma(g) = 0$ ).

The amplitude-frequency characteristics  $\tilde{f}(k)$  ( $k = 2\pi/\lambda$  is the wave number, frequency parameter, or simply frequency,  $\lambda$  stands for the wavelength in free space) we derive from time characteristics  $f(t)$

by applying the integral Fourier transform

$$\tilde{f}(k) = \frac{1}{2\pi} \int_0^T f(t)e^{ikt} dt \leftrightarrow f(t), \tag{5}$$

where  $T$  is the maximum value of the observation time  $t$ .

The internal parameters of the method are: The space-step  $\bar{h} \geq 2\bar{l}$  and the time-step  $\bar{l}$  of the grid in the finite-difference approximation of the original initial boundary-value problems,  $L, M$  (is defined below), and some others. They are determined by a required accuracy and physical interpretation. Thus for example,  $M$  specifies a zone (near-field, intermediate-field or far-field) for which a pattern  $D(\phi, k, M)$  is calculated. We assume that the near-field zone is limited by the value  $M = L$ , while the far-field zone starts from the value of  $M$  such that its further growth does not cause a feasible change in  $D(\phi, k, M)$  for all  $k$  considered.

The near-zone pulsed field  $U(g, t)$  is calculated directly in the domain  $\mathbf{Q}_L$ , while the far-field is determined by translating the field  $U(g, t)$  from the arc  $\rho = L$  onto the arc  $\rho = M > L$ , which is shifted from the boundary  $\mathbf{L}$  for a required distance. This can be done with the help of the exact radiation conditions for outgoing cylindrical waves (3) (see, for example, formulas (3.8) and (3.10) in [3]), which specify a transport operator  $Z_{L \rightarrow \rho}(t)$  such that

$$\begin{aligned} \bar{u}(\rho, t) &= \{\bar{u}_n(\rho, t)\}_n = Z_{L \rightarrow \rho}(t) \left[ \partial \bar{u}(\rho, \tau) / \partial \rho|_{\rho=L}, \bar{u}(L, \tau) \right], \\ \rho &\geq L, t \geq \tau \geq 0. \end{aligned}$$

From the space-time amplitudes  $\bar{u}_n(\rho, t)$  of the field  $U(g, t)$  calculated for a circle  $\rho = L$ , the monochromatic far-field  $\tilde{U}(\rho, \phi, k) \leftrightarrow U(\rho, \phi, t)$  ( $\rho = M > L$ ) can be determined as well. To do this, the following spectral representations should be used

$$\bar{u}_n(\rho, t) \leftrightarrow \tilde{u}_n(\rho, k) = a_n(k) H_n^{(1)}(k\rho), \quad n = 0, \pm 1, \pm 2, \dots, \tag{6}$$

which follow from the partial radiation conditions for outgoing cylindrical waves (see, for example, Formula (1.37) in [3]). First we find the sets of complex amplitudes  $a_n(k)$  and then we obtain  $\tilde{U}(M, \phi, k)$  upon using the radiation conditions.

### 3. ANALYSIS AND SPECTRUM SPARSENESS OF THE RESONATORS OF CLASSICAL CONFIGURATION

The algorithm outlined in Section 2 for solving problem (1) and the approaches suggested and tested in [6, 7] we now use for obtaining such

key resonator spectral characteristics as the eigenfrequencies and the field patterns for resonance oscillations.

Let the confocal resonator depicted in Fig. 1 be excited through the port  $\mathbf{L}_1$  (a section of the input waveguide by the plane  $y = 0$ ) by a pulsed  $H_{01}$ -wave

$$U_1^i(g, t) : v_1(0, t) = 4 \frac{\cos[\tilde{k}(t - \tilde{T})] \sin[\Delta k(t - \tilde{T})]}{t - \tilde{T}} \chi(\bar{T} - t) = F_1(t), \quad \tilde{k} = 8.0, \Delta k = 1.2, \tilde{T} = 25, \bar{T} = 100. \quad (7)$$

Here  $\chi$  is the Heaviside function, while the parameters  $\tilde{k}$ ,  $\Delta k$ ,  $\tilde{T}$ , and  $\bar{T}$  determine the central frequency, bandwidth, delay time, and signal duration, respectively. The total observation time is  $T = 3000$ . The diaphragm bounded from the right by the plane  $y = d$  is of thickness  $\bar{h} = 0.04$ , the coupling aperture dimension equals 0.16. The structure as well as the field  $U(g, t) = E_x(g, t)$  generated in it by signal (7) are symmetric about the plane  $z = 0$ . The signal  $U_1^i(g, t)$  occupies the

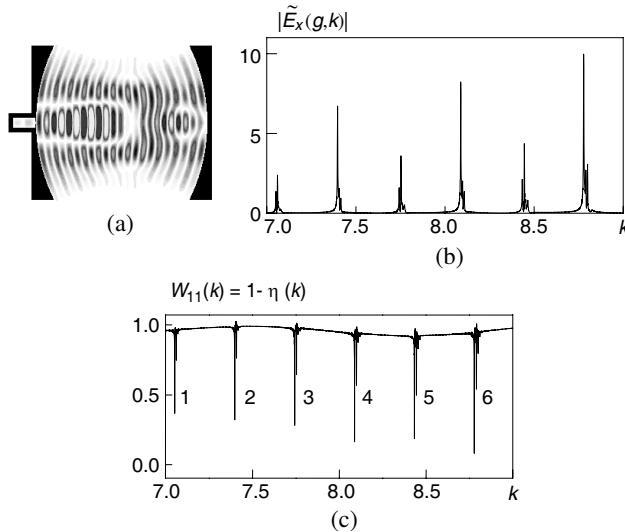


**Figure 2.** Excitation of the resonator by the pulsed  $H_{01}$ -wave (7). (a) The field pattern (spatial distribution of  $E_x(g, t)$ ) at  $t = 2265$ . (b) Spectral amplitudes of the  $E_x$ -component at the point  $g_1 = \{5.5, 0.0\}$ . (c) Relative fraction of energy reflected back into the input waveguide  $W_{11}(k) = 1 - \eta(k)$ ; the resonant frequencies are:  $K_1 \approx 7.05$ ,  $K_2 \approx 7.4$ ,  $K_3 \approx 7.74$ ,  $K_4 \approx 8.09$ ,  $K_5 \approx 8.43$ , and  $K_6 \approx 8.78$ .

frequency band  $6.8 < k < 9.2$ . Within this band we have a beyond-cutoff diaphragm and a single-mode input waveguide  ${}_1\mathbf{Q}$ . The first cutoff points of the waveguide are  $k_1 \approx 5.61$  and  $k_2 \approx 11.22$ . The results of the structure response on this excitation are presented in Fig. 2. The spectral distribution could be inferred by both  $|\tilde{E}_x(g, k)|$  (Fig. 2(b)) and  $W_{11}(k)$  (Fig. 2(c)). However, the function  $W_{11}(k)$  is preferable since it does not depend on the observation point.

The next step is to excite the resonator by a quasi-monochromatic  $H_{01}$ -wave.

$$U_1^i(g, t) : v_1(0, t) = P(t) \cos \left[ \tilde{k} (t - \tilde{T}) \right] = F_2(t),$$

$$\tilde{T} = 0.5, P(t) : 0.1-5-75-80 \tag{8}$$

( $P(t)$ :  $t_1 - t_2 - t_3 - t_4$  is a trapeziform envelope being equal to zero for  $t < t_1, t > t_4$  and to unity for  $t_2 \leq t \leq t_3$ ), whose central frequency  $\tilde{k} = K_j$  ( $j = 1, 2, \dots, 6$ ) coincides with the resonant frequencies determined previously (see Figs. 2(b), (c)). The results for  $k = K_2 \approx 7.4$  are shown in Fig. 3. The data obtained during these

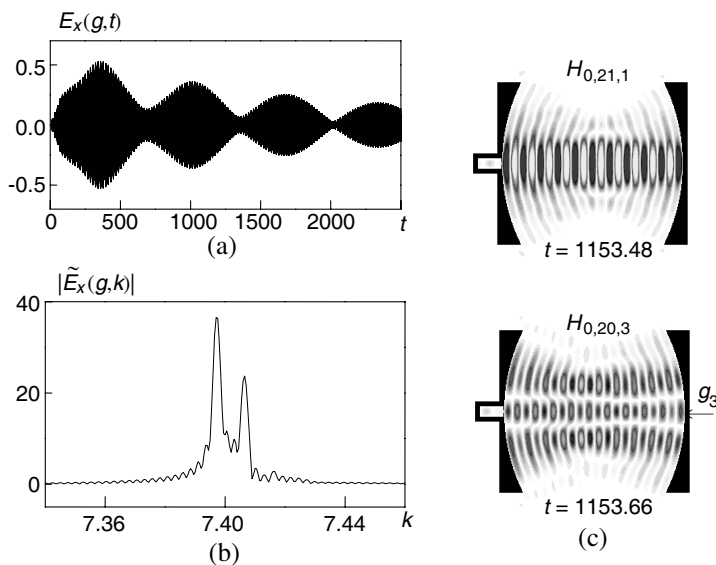


**Figure 3.** The resonator’s response on the quasi-monochromatic  $H_{01}$ -wave (8) with the central frequency  $\tilde{k} = 7.4$ . ((a), (b)) Dynamic and spectral amplitudes of the  $E_x$ -component at the point  $g = g_3$ . (c) Spatial distribution of  $E_x(g, t)$  at  $t = 1153.48$  and  $t = 1153.66$ .

numerical experiments allow us to conclude: 1. In the frequency band  $7.0 < k < 9.0$  the resonator sustains high-Q free  $H_{0,n,1}$ - and  $H_{0,n-1,3}$ -oscillations ( $n = 20, \dots, 25$ ). 2.  $H_{0,n,1}$ - and  $H_{0,n-1,3}$ -oscillations ( $n = 20, \dots, 25$ ) have the eigenfrequencies  $\bar{k}_{n,1}$  and  $\bar{k}_{n-1,3}$  such that  $\text{Re}\bar{k}_{n,1} \approx \text{Re}\bar{k}_{n-1,3} \approx K_{n-19}$ . 3.  $H_{0,n,1}$ - and  $H_{0,n-1,3}$ -oscillations are high-Q oscillations with comparable Q-factors, therefore little can be done to isolate one of them from resonator's response on the broadband signal (7) or narrow-band signal (8) even for high observation times  $t$ .

Let us replace the right-hand mirror with a metal plane reflector  $\chi[y - (R/2 + d)] \chi[(R/2 + d) + 0.2 - y] \chi[b - |z|]$  (Fig. 4). The resonant frequencies of the modified semi-confocal resonator for the resonances 1–6 ( $K_1 \approx 7.08$ ,  $K_2 \approx 7.44$ ,  $K_3 \approx 7.78$ ,  $K_4 \approx 8.13$ ,  $K_5 \approx 8.47$ ,  $K_6 \approx 8.82$ ) are little different from those for the resonator discussed above. The distinction is that the oscillations, whose antinodes fell previously on the symmetry plane  $y = R/2 + d$  of the confocal resonator, disappear from the spectrum. The spectrum crowding does not already observed in the neighborhood of the frequencies  $k \approx K_j$ . All oscillation modes sustained by the semi-confocal resonator ( $H_{0,n,m}$ -oscillations,  $n = 10, 11, 12$ ,  $m = 1, 3$ ) are clearly defined in the responses on the excitation by quasi-monochromatic signals (8) with the central frequencies  $\bar{k} = K_j$  ( $j = 1, 2, \dots, 6$ ) (Fig. 4(c)).

The spectrum can be rarified significantly with abrupt decrease of Q-factors of the  $H_{0,n,3}$ -oscillations through modification of resonator's geometry as it shown in Fig. 5(b): The right-hand plane mirror is replaced by the piecewise-plane reflector whose central section is determined by the field spot dimensions for  $H_{0,n,1}$ -oscillations. The Q-factor of the  $H_{0,n,3}$ -oscillations, which are nominally present in the spectrum of the modified resonator, are governed by the angle  $\beta$ .

A drastic spectrum sparseness in the modified resonator is accomplished by the use of a thin (the thickness is  $\bar{h} = 0.04$ ) metal band being placed along the line of antinodes of the  $H_{0,12,1}$ -oscillations (Fig. 6). It does not distort the  $H_{0,12,1}$ -oscillations and, at the same time, breaks down the  $H_{0,10,1}$ - and  $H_{0,11,1}$ -oscillations (pure spectrum sparseness). The band width ( $2b_2 = 0.28$ ) is much less than the field spot size of the longitudinal oscillations. Because of this, the band can not act as a mirror reducing resonator's volume and giving rise to oscillations with fewer field variations. It is obvious that in order to tune the resonator sustaining in the frequency band  $7.0 < k < 9.0$  the only  $H_{0,12,1}$ -oscillation to the operation mode with  $H_{0,10,1}$ - or  $H_{0,11,1}$ -oscillation, one should only to shift the band along the  $y$ -axis.

An increase in the size  $b$  of the confocal resonator mirrors (Fig. 1 and Fig. 7(a)) up to the value  $b = 5.0$  results in the noticeable growth

of the Q-factor of the oscillations with five field spots on the mirrors. The oscillations  $H_{0,n-2,5}$  ( $n = 20, \dots, 25$ ) have the eigenfrequencies  $\bar{k}_{n-2,5}$  such that  $\text{Re}\bar{k}_{n,1} \approx \text{Re}\bar{k}_{n-1,3} \approx \text{Re}\bar{k}_{n-2,5} \approx K_{n-19}$ . That is why we observe triple resonances in the vicinity of the points  $K_1$  to  $K_6$  in the confocal resonator and double ( $K_1, K_3$ , and  $K_5$ ) or single resonances ( $K_2, K_4$ , and  $K_6$ ) in the semi-confocal resonator (Fig. 7(b)). In this case, too, the use of perfectly conducting bands (of the same size  $0.04 \times 0.28$ ) results in a sparse spectrum in the frequency band  $7 < k < 9$  (Fig. 7(d)).

Similar results we obtain for semi-transparent mirrors as right-hand reflectors, namely, a dielectric mirror ( $\epsilon = 40$ , the mirror thickness equals 0.2) and a grating mirror (Fig. 8). The imaginary parts of the complex eigenfrequencies  $\bar{k}$  corresponding to the isolated oscillations (see also Fig. 7(d)) are evaluated from a behavior of the freely oscillating (once the sources are switched off) field

$$U(g, t) = U(\tau) \approx A \exp(\tau \text{Im}\bar{k}) \cos(\tau \text{Re}\bar{k} + B), \tau = t - t_4 > 0, \quad (9)$$

generated by the quasi-monochromatic  $H_{01}$ -wave (8) with the central

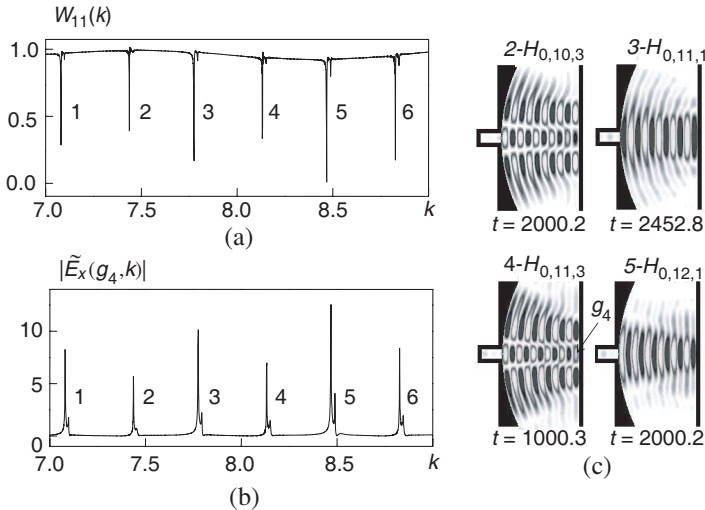


**Figure 4.** Electrodynamics characteristics of a semi-confocal resonator. (a) Relative fraction of energy reflected back into the input waveguide. (b) Spectral amplitudes of the  $E_x(g, t)$ -component at the point  $g = g_4$ . (c) Spatial distribution of  $E_x(g, t)$  when exciting the resonator by the quasi-monochromatic  $H_{01}$ -wave (8) with the central frequencies  $\tilde{k} = 7.44$  (2),  $\tilde{k} = 7.78$  (3),  $\tilde{k} = 8.13$  (4), and  $\tilde{k} = 8.47$  (5).

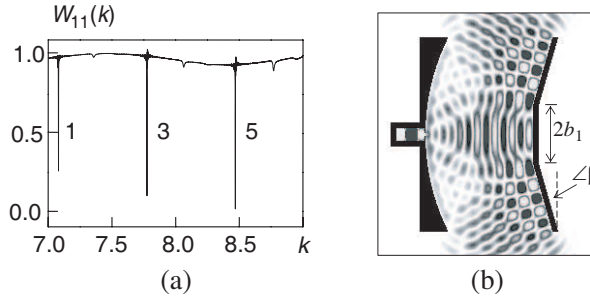


**Figure 5.** The response of the modified resonator ( $b_1 = 1.24$ ,  $\beta = 16^\circ$ ) on the pulsed  $H_{01}$ -wave (7). (a) The function  $W_{11}(k) = 1 - \eta(k)$ . (b) Spatial distribution of  $E_x(g, t)$  at  $t = 32$ .

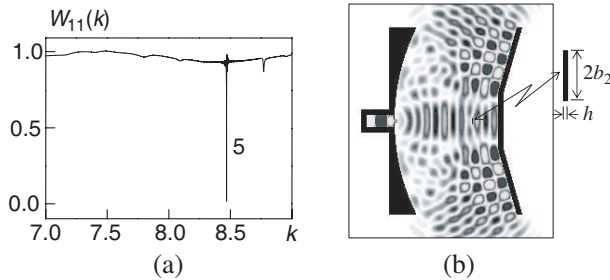


**Figure 6.** A reduction in number of free oscillations in the resonator modified by placing a thin metal band inside. The response of the modified resonator on the pulsed  $H_{01}$ -wave (7). (a) The function  $W_{11}(k) = 1 - \eta(k)$ . (b) The spatial distribution of  $E_x(g, t)$  at  $t = 32$ .

frequency  $\tilde{k} = \text{Re}\bar{k}$  [6, 7]. The observation point  $g$  in (9) is located, as a rule, close to an oscillation antinode, while the minimal signal duration is dictated by the following requirement: Within a frequency band occupied by the signal (8), there must be no values  $\text{Re}\bar{k}_m$  associated with other high-Q free oscillations.

#### 4. QUASIOPTICAL RESONATORS WITH GRATING MIRRORS

Consider some simple resonators with reflecting and semitransparent gratings as dispersive mirrors. Let us determine first spectral characteristics of the structure depicted in Fig. 9(a). This is a Fabry-Perot resonator with parallel perfectly conducting mirrors 0.1 in

thickness. A current source

$$F(g, t) = F_1(t) \chi(4 - |y|) \chi(3 - z) \chi(z - 1),$$

$$\tilde{k} = 6.5, \Delta k = 2.0, \tilde{T} = 50, \bar{T} = 100, T = 500, \quad (10)$$

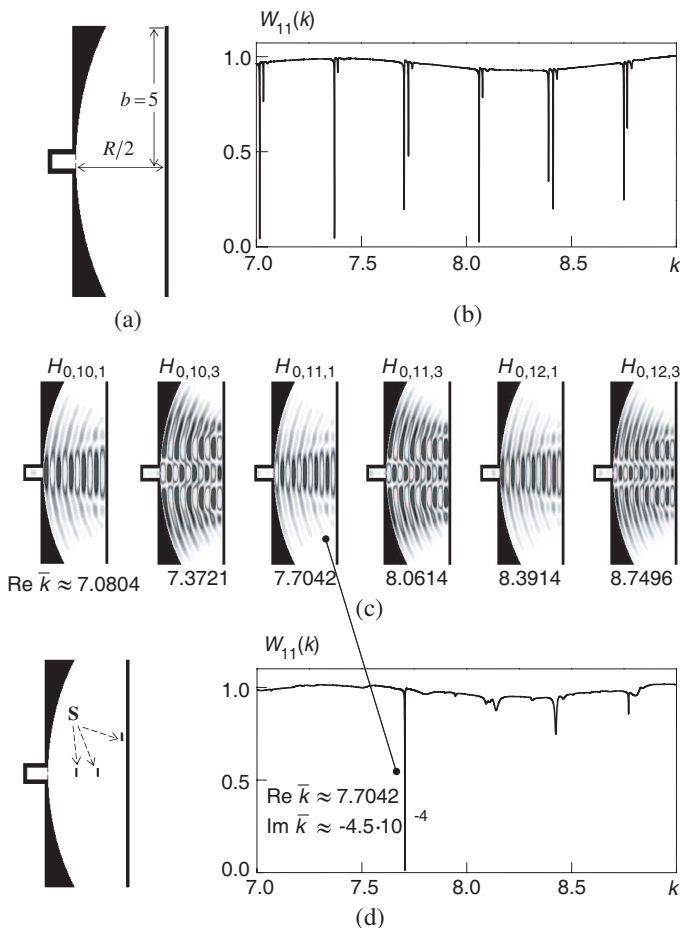


**Figure 7.** (a) A semi-confocal resonator with a plane metal mirror. ((b), (c)) The resonator's spectrum and field patterns. (d) The spectrum sparseness attained by the use of thin metal bands. One of the bands is located at the antinodes of the oscillations  $H_{0,10,3}$ ,  $H_{0,11,3}$ , and  $H_{0,12,3}$ , two others are placed into two nodes of the  $H_{0,11,1}$ -oscillation.

occupying the frequency band  $4.5 < k < 8.5$  excites in the resonator the oscillations symmetric about the principal axis  $y = 0$ , and no other (Fig. 9(c)). One of these oscillations ( $H_{0,1,19}$ ) corresponds to the eigenfrequency  $\bar{k} \approx 7.62 - i0.00178$ . The field pattern as well as the values  $\text{Re}\bar{k}$  and  $\text{Im}\bar{k}$  have been determined from the behavior of the function  $U(\tau) = U(g, t)$  ( $\tau = t - t_4 > 0$ ) for the resonator excited by the narrow-band current source

$$\begin{aligned} F(g, t) &= F_2(t) \chi(4 - |y|) \chi(3 - z) \chi(z - 1), \\ \tilde{k} &= 7.62, \quad \tilde{T} = 0.5, \quad P(t) : 0.1\text{--}5\text{--}190\text{--}195 \end{aligned} \quad (11)$$

(Fig. 9(b) and Fig. 9(d); the curves  $\Gamma^\pm(\tau)$  enveloping the function  $U(\tau)$  are given by the equations  $\Gamma^\pm(\tau) = \pm 0.153 \exp(-0.00178\tau)$ ). In the experiments being discussed in this Section, the observation point is located on the principal axis of the resonator at a distance of a quarter of the wavelength  $\tilde{\lambda} = 2\pi/\tilde{k}$  from the upper mirror. On the axis  $\text{Im}k = 0$ , the elements  $\bar{k}_n$  of the resonator's spectrum  $\Omega_k$  associated with high-Q oscillations are represented by a nearly-equidistant system

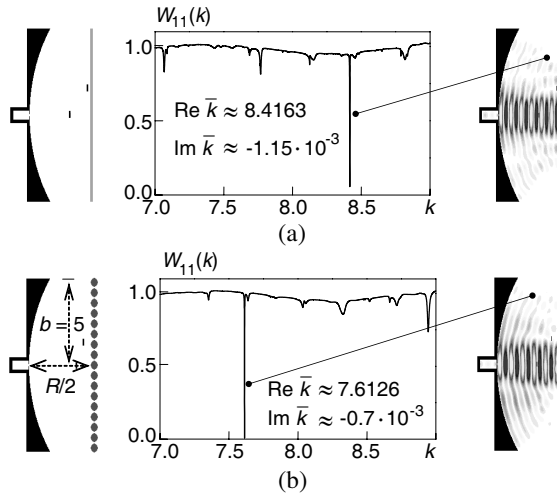


**Figure 8.** (a) Selection of oscillations in the resonator with a dielectric mirror ( $\varepsilon = 40$ ; the centers of the bands are located at the points  $g = \{4.2, 0.0\}$  and  $g = \{5.5, 1.52\}$ ). (b) The same for the resonator with a rod grating ( $\varepsilon = 1$ ,  $\sigma_0 = 5.8 \cdot 10^7$ , the grating period equals 0.6, the rod diameter is 0.45; the centers of the bands are located at the points  $g = \{4.16, 0.0\}$  and  $g = \{5.2, 1.48\}$ ).

of points  $k \approx \text{Re}\bar{k}_n$  (Fig. 9(c)). At these points, the value  $|\tilde{U}(g, k)|$  characterizing magnitude of spectral amplitudes of the field  $U(g, t)$  is determined by the Q-factor of the associated free oscillations together with the function  $C(\tilde{F}, \bar{k}_n)$  (see paper [7]). This function represents the degree of matching of the fields generated by sources and the free oscillation.

A sparse spectrum in the Fabry-Perot resonator can be achieved by replacing nonselective resonator mirrors with grating-mirrors [6]. A model synthesis algorithm [10] based on the so-called prototype principle [2] allows one to forecast the spectrum changes, to determine eigenfrequencies distribution across an operating range, and to obtain field patterns for high-Q oscillations with a required accuracy. Now we dwell briefly on the principle of operation of grating-mirrors in controlled changes of spectral characteristics of an open resonator. As a preliminary we give some well-known data [2, 4, 5].

Let a periodic along the  $y$ -axis grating ( $l$  is the period) located within the layer  $-h \leq z \leq 0$  be excited from the region  $z > 0$  by a plane  $E$ -polarized wave  $\tilde{U}^i(g, k) = \exp[ik(y \sin \alpha - z \cos \alpha)]$  ( $0 \leq \alpha < 90^\circ$ ). A secondary field in the reflection region ( $z > 0$ ) and transmission

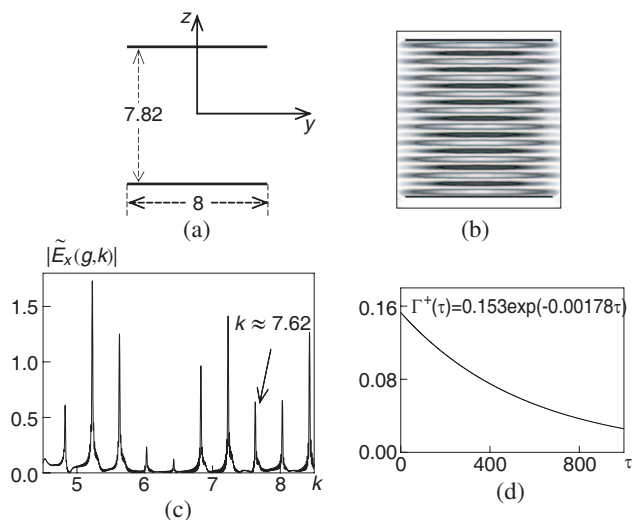


**Figure 9.** (a) A Fabry-Perot resonator. (b) A field pattern for the free oscillation with the eigenfrequency  $\bar{k} \approx 7.62 - i0.00178$ . (c) The response of the resonator on the wideband current excitation (10). (d) The envelope  $\Gamma^+(\tau)$  characterizing the resonator Q-factor.

region ( $z < -h$ )

$$\tilde{U}^s(g, k) = \begin{cases} \sum_{n=-\infty}^{\infty} A_n(k) \exp [i(\Phi_n y + \Gamma_n z)] \\ = \sum_{n=-\infty}^{\infty} \tilde{U}_n^A(g, k), z > 0 \\ \sum_{n=-\infty}^{\infty} B_n(k) \exp [i(\Phi_n y - \Gamma_n(z+h))] \\ = \sum_{n=-\infty}^{\infty} \tilde{U}_n^B(g, k), z < -h, \end{cases}$$

$$\Phi_n = 2\pi n/l + k \sin \alpha, \quad \Gamma_n = \sqrt{k^2 - \Phi_n^2}, \quad \operatorname{Re}\Gamma_n \geq 0, \quad \operatorname{Im}\Gamma_n \geq 0, \quad (12)$$

consists of a finite number of homogeneous (propagating) spatial harmonics  $\tilde{U}_n^A(g, k)$  and  $\tilde{U}_n^B(g, k)$  ( $n$  is such that  $\operatorname{Im}\Gamma_n = 0$ ) outgoing away from the grating at the angles  $\alpha_n = -\arcsin(\Phi_n/k)$  in the reflection zone and at the angles  $\alpha_n = \pi + \arcsin(\Phi_n/k)$  in the grating's transmission zone (all the angles are measured in the plane  $yOz$ , anticlockwise from the  $z$  axis). The angle  $\alpha$  is an angle of incidence of the wave  $\tilde{U}^i(g, k)$ . The values  $W_n^A = |A_n|^2 \operatorname{Re}\Gamma_n/\Gamma_0$  and  $W_n^B = |B_n|^2 \operatorname{Re}\Gamma_n/\Gamma_p$  determine the relative parts of the energy directed by the structure into the corresponding spatial radiation channel. The channel corresponding to the  $n$ -th harmonic, we shall call 'open' if  $\operatorname{Im}\Gamma_n = 0$ . The regime when only one channel is open for spatial harmonics ( $n = 0$ ) we shall call the single-mode regime. For such a regime, the principal spatial harmonic in the reflection zone is referred to as specular harmonic, and its amplitude ( $A_0$ ) is said to be the reflection coefficient (obviously,  $B_0$  is called the transmission coefficient).

The angle between the propagation directions of the primary and the minus  $m$ -th reflected plane wave  $\alpha - \alpha_{-m} = 2\beta$  is determined from the equation  $kl \sin(\alpha - \beta) \cos \beta = \pi m$ . Particularly, at  $\beta = 0$  or at  $kl \sin(\alpha) = \pi m$  the harmonic  $\tilde{U}_{-m}^A(g, k)$  propagates towards the incident wave. The occurrence of such a nonspecular reflecting mode is called autocollimation. If, in addition, we have  $W_{-m}^A(k) \approx 1$ , then we are dealing with a total autocollimation reflection phenomenon.

The propagation direction and the energy of homogeneous harmonics of the secondary field depend on their number  $n$  and on the values of  $k$  and  $\alpha$ . Therefore, grating mirrors, as distinct from regular mirrors, differently respond to the waves that generate oscillations of different kind and frequency. This ability of grating-mirrors can be efficiently used when solving the problems of controlled changes of basic spectral characteristics of open quasi-optical resonators. The preceding is supported by the following example.

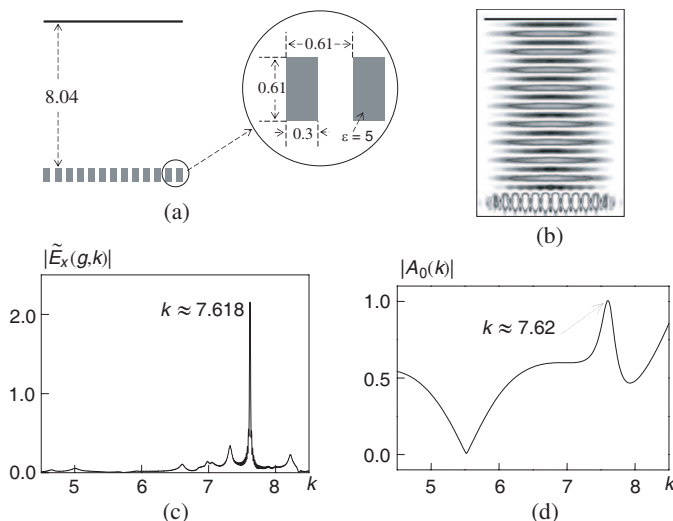


**Figure 10.** (a) A resonator with a grating-mirror. (b) The field pattern of the oscillation with the eigenfrequency  $\bar{k} \approx 7.618 - i0.0034$ . (c) Spectral amplitudes of the field  $E_x(g, t)$  excited in the resonator by the wideband current source (10). (d) The absolute value of the grating reflection coefficient.

An infinite semi-transparent dielectric grating, a period of which is shown in Fig. 10(a), totally reflects a normally incident ( $\alpha = 0$ ) plane  $E$ -polarized wave at the frequency  $k = K_1 \approx 7.62$ ; in this case we have  $|A_0(K_1)| = 1$  and  $\arg A_0(K_1) = 0.163$ . The absolute value of the reflection coefficient  $A_0(k)$  exceed 0.7 only in two narrow frequency bands, namely, close to the point  $k = K_1$  and at the end of the range  $4.5 < k < 8.5$  (Fig. 10(d)). At the other points (where only first harmonics of the secondary field propagate), the most part of the energy is concentrated in the transmitted plane wave  $\tilde{U}_0^B(g, k)$ . At the frequency  $k = K_1$ , the Fabry-Perot resonator (Fig. 9) sustains the free oscillation whose partial waves are incident near-normally on the plane metal mirrors and reflected by them without noticeable reduction in the amplitude absolute value. The amplitude sign changes to the opposite. Therefore, it may be asserted that at the frequency  $k = K_1$  a resonator mirror made from a semitransparent dielectric grating will operate in the same manner as an ordinary metal mirror. It is essential that the difference between the reflection coefficient phases for a grating and a metal plane should be compensated by varying a distance between resonator's mirrors. Really, the resonator modified

correspondingly (Fig. 10(a)) sustains at the frequency  $k \approx K_1$  the same  $H_{0,1,19}$ -oscillation (Figs. 10(b),(c)) as the prototype-resonator does (Fig. 9(b)). The oscillation's eigenfrequency  $\bar{k} \approx 7.618 - i0.0034$  (Fig. 10(c)) differs from the prototype's one only slightly. A spectrum of the modified resonator is substantially sparse (compare Fig. 10(c) and Fig. 9(c)). An important point is that this result can be predicted with certainty basing on the behavior of the function  $A_0(k)$  in the frequency range  $4.5 < k < 8.5$ .

If  $k < 2\pi/l(1 + |\sin \alpha|)$ , then the only propagating harmonic  $\tilde{U}_0^A(g, k) = A_0(k) \exp[i(\Phi_0 y + \Gamma_0 z)]$  exists in the secondary field (12) generated by perfectly conducting reflecting gratings (the single-mode regime), where  $A_0(k) = \exp(i \arg A_0(k))$ . That is the reason why in the range  $4.5 < k < 2\pi/l \approx 5.51$  the spectra of the Fabry-Perot resonator (Fig. 9) and the resonator whose bottom mirror is a segment of a rectangular echelette (Fig. 11) differ little in a qualitative sense. The variations in the values of  $\text{Re} k_n$  are determined by  $\arg A_0(k)$ , which is a function of frequency and geometric parameters of the grating. However, beyond the threshold point  $k \approx 5.51$  (the point beyond which higher harmonics  $\tilde{U}_{\pm 1}^A(g, k)$  arise in the secondary field

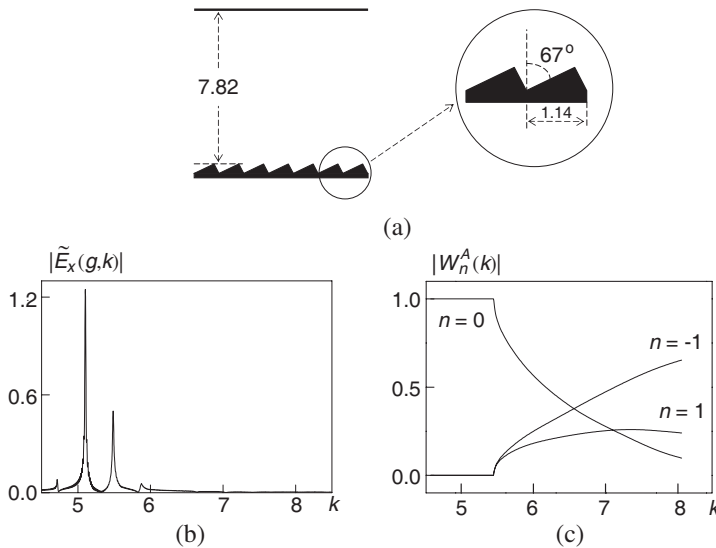


**Figure 11.** (a) A resonator with a reflecting grating. (b) Spectral amplitudes of the field  $E_x(g, t)$  excited in the resonator by the wideband current source (10). (c) The energy content of the harmonics  $\tilde{U}_n^A(g, k)$ ,  $n = 0, \pm 1$ .

at  $\alpha = 0$ ), the modified resonator no longer sustains high-Q free oscillations (Fig. 11(b)). This is caused by the increase for  $5.51 < k < 8.5$  of the part of energy  $W_{\pm 1}^A(k)$  that is directed by the echelette into plane waves  $\tilde{U}_{\pm 1}^A(g, k)$  (Fig. 11(c)) outgoing from the grating at angles  $40.4^\circ < |\alpha_{\pm 1}(k)| < 90^\circ$ . Therefore, oscillation reduce substantially and a major portion of the incident energy is directed into free space out of the resonator.

Consider now a space bounded by two parallel reflectors as it shown in Fig. 12(a). It is evident that in the case of plane mirrors this resonator does not sustain high-Q oscillations. The only way to force the resonator to do this is to replace its flat mirrors by the gratings that reflect plane waves in a direction opposite to the incidence direction.

For an infinite metal grating from which the mirrors of the resonator shown in Fig. 12(a) are made, the efficiency of reflection into the minus first autocollimating harmonic (propagating in a direction opposite to the incidence) approaches 1 in a frequency range  $5.25 < k < 7.25$  (see Fig. 133 in [5]:  $kl \sin(\alpha) = \pi$ ,  $W_{-1}^A(k) \approx 1.0$ ). In this frequency range, the incident plane wave  $\tilde{U}^i(g, k)$  and the reflected plane wave  $\tilde{U}_{-1}^A(g, k)$  are deflected from the grating normal through an

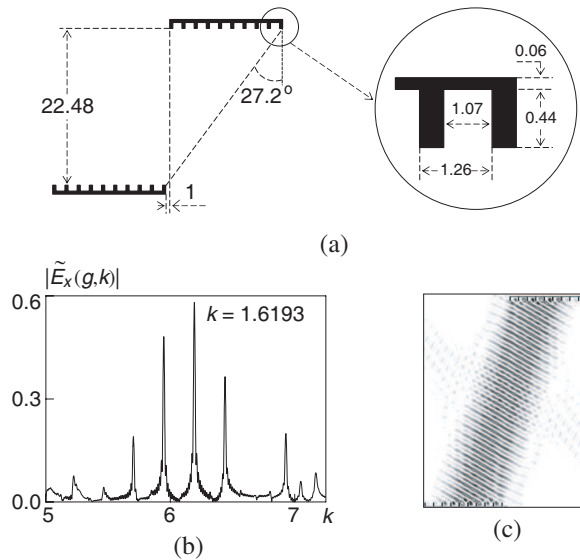


**Figure 12.** (a) Geometry of the resonator. (b) The resonator response on a wideband current source. (c) The field pattern of the oscillation with the eigenfrequency  $\bar{k} = 6.193 - i0.00265$ .

angle  $20.16^\circ < \alpha(k) < 28.35^\circ$ . Obviously, high-Q free oscillations may occur in the structure only in the vicinity of the point  $k = 5.45$ . This frequency corresponds to the angle  $\alpha(k) = 27.2^\circ$ , i.e., to the inclination of the resonator principal axis. The calculated spectral characteristics confirm our assumption. This is illustrated in Fig. 12(b) by spectral amplitudes of the field  $E_x(g, t)$  excited in the resonator by a broadband current source like that given by (10). The source occupies a space of  $5.8 \times 10.6$  and is located at the resonator geometric center being directed across its principal axis. A field pattern for the oscillation with the eigenfrequency  $k = 6.193 - i0.00265$  is shown in Fig. 12(c). The field spot is not practically found close by two farthest periods of the grating: The structure operates as a resonator whose principal axis is inclined at an angle of  $\beta \approx 24^\circ$ . As a traveling direction of partial waves of the oscillation, this value agrees well with the value  $\text{Re} \bar{k} = 6.193$ .

## 5. CONCLUSION

The demands for controlled changes of spectral characteristics of open resonant structures as well as for synthesis of resonators sustaining oscillations with a given field pattern and Q-factor arises when solving applied radiophysical problems involved in the design of solid-state generators, resonant antennas (for example, [11]), power compressors, and radiators of short high-power radio pulses (for example, [12]). A lot of instructions furnishing, in the authors opinion, the desired results are available in the literature. Unfortunately, for the most part, these directions are qualitative in character without experimental or theoretical support. In the present work, we have estimated for the first time the actual efficiency of various ways for controlled changes in spectra of open quasi-optical resonators; we have used for this purpose mathematical models providing a reliability of physical results.

## REFERENCES

1. Weinstein, L. A., *Open Resonators and Open Waveguides*, Golem Press, Boulder, CO, 1969.
2. Shestopalov, V. P. and Y. K. Sirenko, *Dynamic Theory of Gratings*, Naukova Dumka, Kiev, 1989 (in Russian).
3. Sirenko, Y. K., S. Strom, and N. P. Yashina, *Modeling and Analysis of Transient Processes in Open Resonant Structures: New Methods and Techniques*, Springer, New York, 2007.

4. Petit, R. (ed.), *Electromagnetic Theory of Gratings*, Springer, New York, 1980.
5. Shestopalov, V. P., A. A. Kirilenko, S. A. Masalov, and Y. K. Sirenko, *Resonance Wave Scattering*, Vol. 1, Diffraction Gratings, Naukova Dumka, Kiev, 1986 (in Russian).
6. Sirenko, Y. K., L. G. Velychko, and F. Erden, "Time-domain and frequency-domain methods combined in the study of open resonance structures of complex geometry," *Progress In Electromagnetics Research*, PIER 44, 57–79, 2004.
7. Velychko, L. G., Y. K. Sirenko, and O. S. Velychko, "Time-domain analysis of open resonators. analytical grounds," *Progress In Electromagnetics Research*, PIER 61, 1–26, 2006.
8. Taflove, A. and S. C. Hagness, *Computational Electrodynamics: The Finite-difference Time-domain Method*, Artech House, Boston, 2000.
9. Sirenko, K. Y. and Y. K. Sirenko, "Exact 'absorbing' conditions in the initial boundary-value problems of the theory of open waveguide resonators," *Comput. Math. Math. Phys.*, Vol. 45, No. 3, 490–506, 2005.
10. Velychko, L. G. and Y. K. Sirenko, "A model synthesis of grating absorbing and pattern-forming structures," *Electromag. Waves Electron. Syst.*, Vol. 7, No. 2, 45–59, 2002 (in Russian).
11. Guerin, N., S. Enoch, G. Tayeb, P. Sabouroux, P. Vincent, and H. Legay, "A metallic Fabry-Perot directive antenna," *IEEE Trans. on Antennas and Propagation*, Vol. 54, No. 1, 220–224, 2006.
12. Tantawi, S. G., R. D. Ruth, A. E. Vlieks, and M. Zolotarev, "Active high-power RF pulse compression using optically switched resonant delay lines," *IEEE Trans. on Microwave Theory and Techniques*, Vol. 45, No. 8, 1486–1492, 1997.